



Brain-wide interactions during hippocampal sharp wave ripples

Noam Nitzan^a , Rachel Swanson^a, Dietmar Schmitz^{b,c} , and György Buzsáki^{a,d,1}

Edited by Edvard Moser, Norges teknisk-naturvitenskapelige universitet, Trondheim, Norway; received January 25, 2022; accepted April 5, 2022

During periods of disengagement from the environment, transient population bursts, known as sharp wave ripples (SPW-Rs), occur sporadically. While numerous experiments have characterized the bidirectional relationship between SPW-Rs and activity in chosen brain areas, the topographic relationship between different segments of the hippocampus and brain-wide target areas has not been studied at high temporal and spatial resolution. Yet, such knowledge is necessary to infer the direction of communication. We analyzed two publicly available datasets with simultaneous high-density silicon probe recordings from across the mouse forebrain. We found that SPW-Rs coincide with a transient brain-wide increase in functional connectivity. In addition, we show that the diversity in SPW-R features, such as their incidence, magnitude, and intrahippocampal topography in the septotemporal axis, are correlated with slower excitability fluctuations in cortical and subcortical areas. Further, variations in SPW-R features correlated with the timing, sign, and magnitude of downstream responses with large-amplitude SPW-Rs followed by transient silence in extrahippocampal structures. Our findings expand on previous results and demonstrate that the activity patterns in extrahippocampal structures depend both on the intrahippocampal topographic origin and magnitude of hippocampal SPW-Rs.

memory | sleep | replay

Exchange of neuronal information occurs in both space and time. As in human speech, messages are conveyed in chunks or frames. The meaning of messages is interpretable only when the entire frame (e.g., sentence) is transmitted, because even the last word can change the intended meaning. Communication between the hippocampus and its target structures occurs in such frames, including theta cycles of online and sharp wave ripples (SPW-Rs) of offline brain states (1). In each temporal frame, distributed neurons across a large spatial segment might be active. For example, during a single theta cycle, neurons from the septal to temporal end of the hippocampus are recruited in a temporal sequence (2, 3). The spatial recruitment of neurons in the hippocampus during SPW-Rs is more complex, varying both in spatial extent and travel direction (3). A neocortical “observer” structure may therefore receive different messages from different hippocampal segments and at different times (4). The varying degrees of spatial recruitment of hippocampal neurons may be broadcast to few or several neocortical targets. In the reverse neocortical-hippocampal routes, similar segmentation rules may apply (1, 5). How the functional topographic relationship between different segments of the hippocampus and brain-wide target areas affect this bidirectional communication has not been studied with sufficiently high temporal and spatial resolution.

Monitoring the interaction between the hippocampus and partner structures would, ideally, require simultaneous recordings along the long axis of the hippocampus and across large neocortical areas and subcortical areas. Toward this goal, a seminal study by Logothetis et al. (6) combined single-site electrophysiological recording in the hippocampus with brain-wide MRI in primates and examined blood-oxygen level-dependent (BOLD) activity surrounding hippocampal SPW-Rs. The results of this study indicated a robust increase in BOLD signal in nearly all cortical areas, paralleled by significant decrease in subcortical areas including the thalamus, midbrain, and basal ganglia. Further analysis indicated a stereotypic time course, with initial suppression of thalamic activity before the onset of SPW-Rs, followed by an activation of prefrontal and midline cortices, then the hippocampus, and finally, activation of sensory cortices (6). In another approach, single-site dorsal hippocampal recordings in the mouse were combined with voltage imaging of the neocortex and found support for both directions of communication (7). However, interpretation of these results is hampered by the slow time course of the BOLD signal and the lack of ground truth for its relationship to spiking activity (8). Moreover, accumulating evidence from neurophysiological recordings in a variety of brain areas [reviewed in (9)] is in conflict with some of the reported BOLD responses. Furthermore, unique patterns of hippocampal spiking activity, even from a single site, are associated with distinct cortical activity patterns

Significance

Bidirectional communication between the hippocampus and other brain areas via sharp wave ripples (SPW-Rs) has been hypothesized to play an important role in cognitive functions. However, brain-wide coupling to SPW-Rs has been difficult to study at high temporal and spatial resolution. Here, we show that SPW-Rs coincide with transient brain-wide increase of functional connectivity. The diversity in SPW-R features was related to slower excitability fluctuations in cortical and subcortical areas. In return, SPW-Rs correlated with the timing, sign, and magnitude of partner structure responses. Our findings provide the most extensive survey of spiking activity surrounding hippocampal SPW-Rs to date.

Author affiliations: ^aNeuroscience Institute, Langone Medical Center, New York University, New York, NY 10016; ^bCharité-Universitätsmedizin Berlin, Corporate member of Freie Universität Berlin, Humboldt-Universität zu Berlin, and Berlin Institute of Health, 10117 Berlin, Germany; ^cNeuroscience Research Center, Charité-Universitätsmedizin Berlin, 10117 Berlin, Germany; and ^dDepartment of Neurology, Langone Medical Center, New York University, New York, NY 10016

Author contributions: N.N. and G.B. designed research; D.S. contributed new reagents/analytic tools; N.N. analyzed the data with input from R.S.; and N.N., R.S., and G.B. wrote the paper.

The authors declare no competing interest.

This article is a PNAS Direct Submission.

Copyright © 2022 the Author(s). Published by PNAS. This article is distributed under Creative Commons Attribution-NonCommercial-NoDerivatives License 4.0 (CC BY-NC-ND).

¹To whom correspondence may be addressed. Email: gyorgy.buzsaki@nyulangone.org.

This article contains supporting information online at <http://www.pnas.org/lookup/suppl/doi:10.1073/pnas.2200931119/DCSupplemental>.

Published May 13, 2022.

(8, 10–13). This assumed local heterogeneity can be ascribed to the distinct spatial origins of SPW-Rs along the septotemporal axis (13, 14) and to other sources of variability, such as SPW-R amplitude, duration, intrahippocampal propagation, and brain state. However, the possibility that different hippocampal segments communicate relatively selectively with other brain targets and, in the reverse direction, that distinct brain structures can differentially affect neuronal activity in different hippocampal segments has not yet been addressed.

To provide a better understanding of the hypothesized spatiotemporally precise interaction between the hippocampus and the numerous extrahippocampal structures, we analyzed the spiking activity of simultaneously recorded neurons by multiple Neuropixels probes from a large number of brain areas in head-fixed mice (15, 16). We identified multiple sources of variability influencing the putative interaction between hippocampal and extrahippocampal regions during SPW-Rs, including the magnitude of SPW-Rs, intrahippocampal propagation of activity, functional topographical relationships, the instantaneous network state in the partner region, and global brain-state changes. These findings demonstrate that SPW-Rs provide highly flexible communication between the hippocampus and other brain regions and highlight the need for brain-wide monitoring of spiking activity to properly identify the sources of variability.

Results

To examine the interaction between the hippocampus and extrahippocampal brain areas with high spatiotemporal precision, we leveraged publicly available datasets (15, 16) that monitored spiking activity across the mouse brain via simultaneous Neuropixels silicon probe recordings in awake head-fixed mice (Fig. 1*A*). For each session, we identified the recording channel with the largest power in the 110- to 250-Hz band of the CA1 pyramidal layer (17) and computed unit firing in hippocampal and other brain regions. To be comparable with functional imaging studies, responses were averaged across all units from the same brain area, unless otherwise noted. We first examined intrahippocampal features of SPW-Rs and then explored their interactions with brain-wide cortical circuits.

Cooperativity of Intrahippocampal Subcircuits During SPW-Rs. In the Allen Institute (AI) dataset, six Neuropixels probes were inserted into targeted visual areas (15) and penetrated distinct hippocampal locations in each experiment. Prior to cranial window implantation, animals underwent intrinsic signal imaging to map the different visual areas and ensure systematic targeting across individual subjects. Probes were coated with fluorescent dye, and probe tracks were reconstructed in three dimensions using an optical projection tomography scanner. These data allowed us to compare neuronal activity underlying SPW-Rs at different septotemporal locations (Fig. 1*A*). SPW-Rs were separately detected on each probe (*Materials and Methods*), and their rate was strongly anticorrelated with running speed and pupil size, confirming previous studies (SI Appendix, Fig. S1) (18). Electrode A was located in the most anterior (septal) part of the dorsal CA1, whereas electrode D was in the most posterior (or temporal part, corresponding to the main curve of the C-shaped hippocampus). Electrodes B, C, and E occupied intermediate segments. Electrode S was most medial and was recorded primarily from the subiculum (Fig. 1*A*; see *Materials and Methods* for the original AI labels).

Several measured parameters showed a systematic change along the septotemporal axis (Fig. 1*B*). Both the magnitude of

ripple power and the magnitude of sharp waves detected in the stratum radiatum were largest in the most posterior sites (D, E) and were decreased toward septal locations (Fig. 1*B*). Ripple frequency similarly increased in the septotemporal direction, whereas the duration of SPW-Rs was longer at more septal sites. We also calculated the fraction of SPW-Rs in which a given CA1/subiculum neuron fired and found that neurons at more posterior sites tended to participate in more SPW-R events than at other sites (Fig. 1*B*). Using peri-SPW-R spike times at the most septal site (A) as a reference revealed that, on average, unit discharges at the more posterior sites occurred earlier than at the septal sites (Fig. 1*C*; probe B: 0 ± 0.4 ms; probe C: 1 ± 0.9 ms; probe D: 1 ± 1.5 ms; probe E: 2 ± 1.7 ms; probe S: 1 ± 1.4 ms; median \pm median absolute deviance [MAD]). This finding was corroborated by analyzing the time offsets of ripple power across electrodes (SI Appendix, Fig. S1 and Movie S1). Ripple wave-related firing (~6-ms synchrony) was coherent at neighboring sites but decreased rapidly with distance (Fig. 1*D*) (14).

SPW-R parameters varied systematically as a function of ripple power. To quantify this effect, we divided SPW-Rs into eight groups based on their ripple power octile (SI Appendix, Fig. S1). Ripple power positively correlated with the magnitude of sharp wave sink, ripple frequency, and SPW-R duration, as well as with the synchrony of both CA1 and CA3 neurons, measured as the fraction of neurons active during SPW-Rs (SI Appendix, Fig. S1). Further, SPW-R magnitude was significantly correlated with several brain-state measures such as pupil diameter, power-spectrum slope (19), and a state index (i.e., “silence density”; see *Materials and Methods*) (20) (SI Appendix, Fig. S1).

It has been illustrated but not quantified that SPW-R power is correlated with the degree of SPW-R spread across the septotemporal axis (14). To address this hypothesis, we detected SPW-Rs separately on each of the six probes using the same threshold and classified events based on the number of probes each event was concurrently detected on. The relative fraction of isolated to global SPW-Rs was similar across probes (SI Appendix, Fig. S2). As expected, ripple power–power correlation was high at neighboring probes, and this correlation decreased with increasing intershank distance (Fig. 2 *A–C* and SI Appendix, Fig. S2). The spatial synchrony of SPW-Rs (i.e., the number of hippocampal recording sites on which a SPW-R was detected) positively correlated with ripple power (Fig. 2*D*). In turn, as expected from the spatial synchrony versus power relationship, spatial synchrony positively correlated with the magnitude of sharp wave sink, ripple frequency, and SPW-R duration, as well as with the synchrony of both CA1 and CA3 neurons, measured as the fraction of neurons emitting at least one spike during SPW-R (Fig. 2 *E–I*). The regression between spatial synchrony and temporal synchrony of SPW-Rs was steeper in CA1 compared to the CA3 region (regression line slope ratio CA1/CA3 = 1.64), implying that the CA1 circuit does not simply respond to but amplifies the CA3 input during SPW-R events (21). The intrahippocampal events were also related to other brain-state variables. The spatial synchrony of SPW-Rs was inversely correlated with the slope of the power spectrum, brain-state index and pupil diameter (Fig. 2 *J–L*), as might be expected from the ripple power relationship with these same variables (18).

Global Brain-Hippocampal Interactions During SPW-Rs. We next investigated extrahippocampal activity surrounding SPW-Rs. For this, we included the University College London (UCL) dataset (16), which contained recordings across a greater

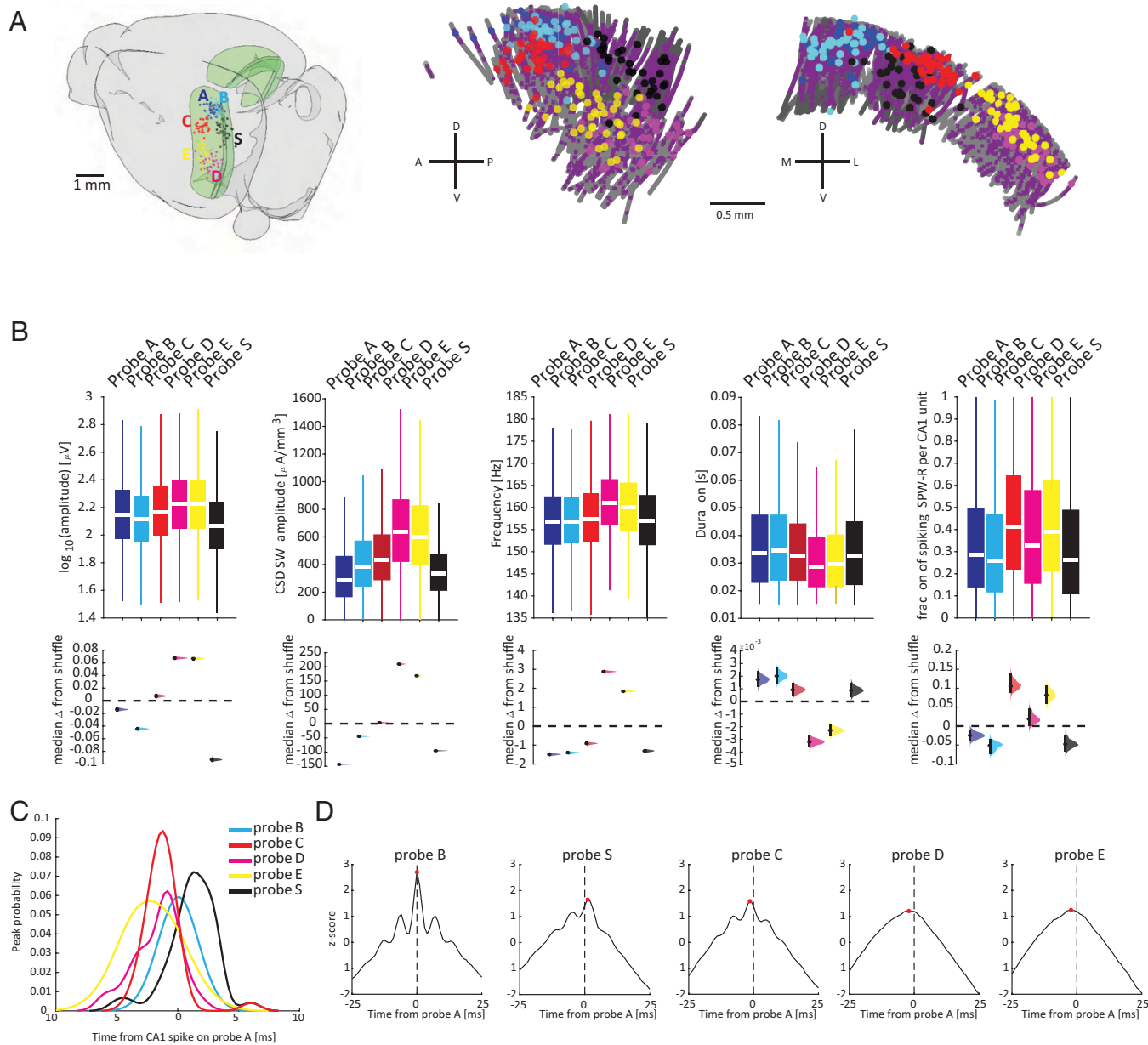


Fig. 1. Ripple features vary along the hippocampal longitudinal axis. (A) Locations of Neuropixels probes from all sessions, color-coded according to probe identity. In each experiment, probes were positioned in a stereotypic manner (15). Probes A–C spanned the dorsal CA1, and D and E were placed in intermediate (posterior) CA1. Probe S was either in the subiculum (19 sessions) or distal CA1 bordering the subiculum (13 sessions). Middle and Right: The recording sites in the CA1 pyramidal layer, shown in the septotemporal and the mediolateral projections, color-coded as in the Left panel. Purple Xs depict the position of individual units. A, anterior; D, dorsal; P, posterior; V, ventral; M, medial; L, lateral; CSD, Current Source Density; SW, Sharp Wave. (B) From Left to Right: Distributions of ripple amplitude, sharp wave amplitude, ripple frequency, ripple duration, and fraction of SPW-Rs in which a given neuron fired at least once ($n = 347,525$ SPW-R events from 50 sessions). Bottom: Effect size estimates depicted as the distribution of differences between the medians of a given probe computed from 5,000 bootstrapped resamples and the median of the values after shuffling the probe labels. Black bars depict 95% CIs. (C) Distribution of spiking peak lags referenced to probe A obtained from cross-correlations between CA1/subiculum spikes on other probes. (D) Averaged (mean \pm SEM) cross-correlograms between CA1/subiculum units on different probes used to calculate the distributions in C, ordered from left to right according to the distance from probe A. Red dot depicts average peak lag.

number of cortical and subcortical sites but, unlike the AI dataset, captured hippocampal activity at fewer locations along the septotemporal axis per recording session (Fig. 3 A and B and *SI Appendix*, Table S1). Across the two datasets, SPW-R response profiles were qualitatively similar (*SI Appendix*, Fig. S3). In our analyses, we only included brain regions with at least 20 recorded neurons and sessions with at least 100 SPW-Rs (separated by at least 500 ms). We found heterogeneous responses across brain areas, but with systematic groupings. Robust short-time (± 50 ms from ripple peak power) modulations in population firing rates were confined mainly to brain structures

monosynaptically connected to the hippocampal-subiculum-entorhinal circuit (Fig. 3 C and D), including prefrontal cortical areas (22), the retrosplenial cortex (12, 23), and the hippocampal continuation taenia tecta, a part of the olfactory cortex (24, 25). In most target regions (but not in the medial septum and thalamus), positively modulated neurons were the majority (Fig. 3D). In contrast to these transient short-time scale responses, the majority of regions shared a common longer time scale modulation. Average population activity began decreasing hundreds of milliseconds before the SPW-R and changed its sign around SPW-R time, suggesting phase locking of SPW-R to

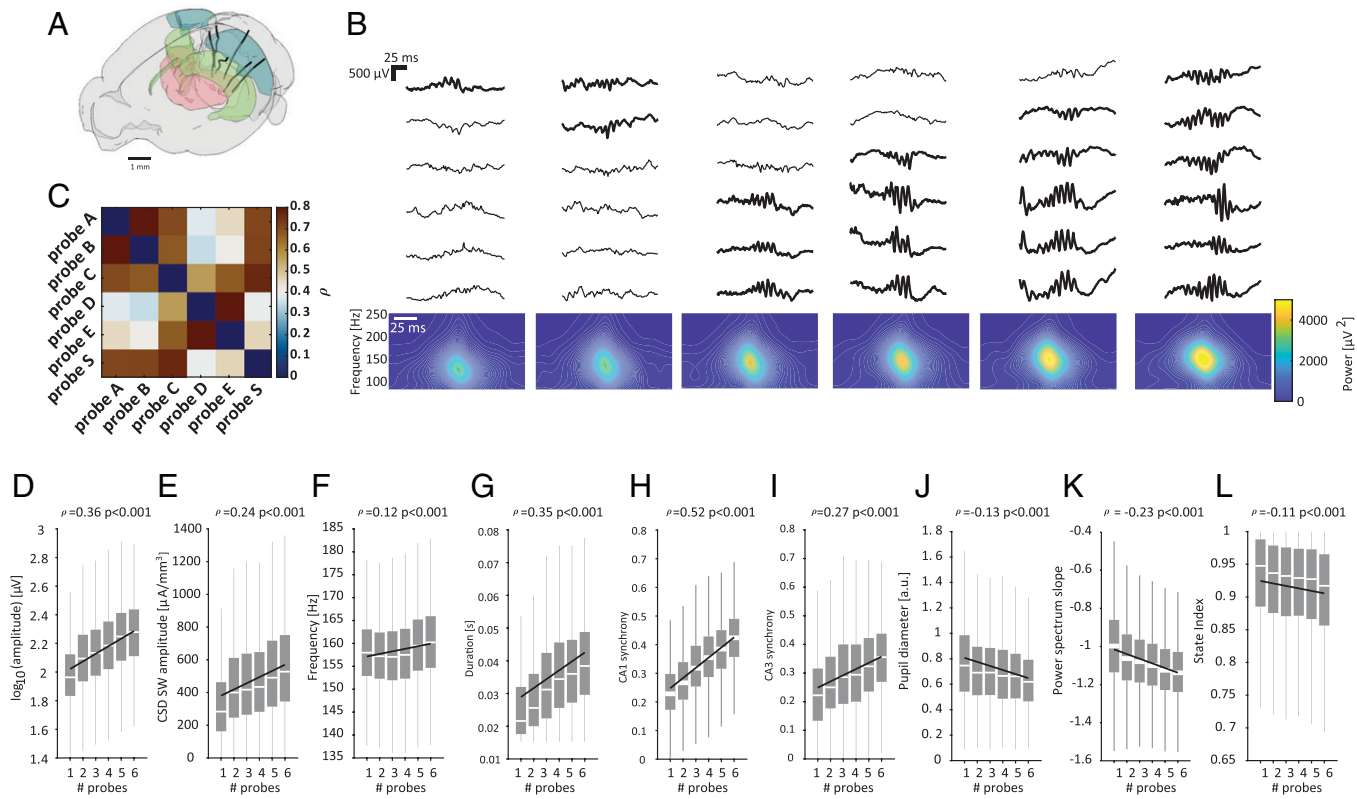


Fig. 2. Ripple features vary as a function of intrahippocampal synchronization. (A) Cartoon showing probe locations in one example session. Hippocampus, green; visual cortex, cyan; thalamus, red. (B) Example raw traces (Top) and average spectrograms (Bottom) for SPW-Rs detected on 1–6 probes from one session. (C) Ripple power peak correlation from all pairs of electrodes averaged across all sessions where all six probes were available ($n = 224,083$ events from 26 sessions). (D–L) Distribution of various SPW-R parameters for SPW-Rs detected on 1–6 probes. Data are displayed as box plots representing median, lower, and upper quartiles and whiskers representing most extreme data points. (J–L) Same as D–I but for various behavioral parameters and brain-state estimators. a.u., arbitrary units; CSD, Current Source Density; SW, Sharp Wave.

slower fluctuations in brain-wide activity. The slow-time scale shift in firing rate was most prominent in the recorded thalamic nuclei but was present in other regions as well (Fig. 3 C and D). To better estimate the short-time scale relationship between brain regions, for each unit we calculated the center of mass (COM) of the SPW-R-triggered peri-event time histogram (PETH). COM distributions for hippocampal subregions matched known synaptic connectivity, with CA3 leading (-20 ± 19 ms, median \pm MAD), followed by CA1 (-9 ± 16 ms) and dentate gyrus (-6 ± 19 ms), while subiculum units displayed more delayed responses (3 ± 16 ms; Fig. 3E). Average delays in extrahippocampal regions lagged behind the hippocampus (Fig. 3F).

To explore the possible routes of hippocampal SPW-R modulation in extrahippocampal regions, we examined fiber projections from all hippocampal subregions using the dataset from the Allen Brain Institute Connectivity Atlas (<https://connectivity.brain-map.org/>; $n = 19$ experiments) and calculated the average fiber density of hippocampal projections to target areas. We found reliable correlation between anatomical connectivity and SPW-R modulation of neurons in most target regions (SI Appendix, Fig. S4). For the remainder of the analyses, we excluded data from UCL recordings (16) because these experiments were designed for active tasks for short recording sessions, and the recording sites varied from experiment to experiment. We first confirmed previous findings (26) regarding ripple and theta phase modulation of neurons in hippocampal and extrahippocampal regions and demonstrated differential ripple-phase locking of deep and superficial CA1 pyramidal neurons (SI Appendix, Fig. S5).

Because the dataset we analyzed also contained visual stimulation epochs, we also examined how functional connectivity between neurons in the hippocampus and other brain areas changed during externally driven (visual stimulation) versus internally organized (SPW-R) states. We computed the mutual information (MI) between the combined multiunit activity (MUA) from pairs of brain regions during either drifting grating visual stimulation or hippocampal SPW-Rs. The MI measure expresses the amount of information that is provided by one variable about another. In contrast to linear correlation, MI shows an increase in information also when the activity of neurons is anticorrelated or nonlinearly related (27). We computed the change in MI in a peri-event window compared to a baseline period (200 to 500 ms prior to visual stimulation or SPW-R) and constructed Δ MI adjacency matrices, which were averaged across sessions and converted into weighted graphs (Fig. 4 A and B). The graph obtained during visual stimulation reflected the expected transfer of information between visual thalamic and cortical areas (15), which formed one strong functional network during stimulus presentation, with only marginal links to the subiculum and dentate gyrus. In contrast, during SPW-Rs, MI increased between hippocampal and visual areas and between hippocampal and thalamic areas but not between cortical and thalamic areas, suggesting a functional segregation of these networks during sensory disengagement and self-organized SPW-R activity (6) (Fig. 4C). To examine the interregional organizing role of SPW-Rs in more depth, we computed the peri-SPW-R Δ MI for consecutive 100-ms windows surrounding SPW-R peaks (referenced to a -500 to -400 ms baseline) between pairs of neurons, yielding nine

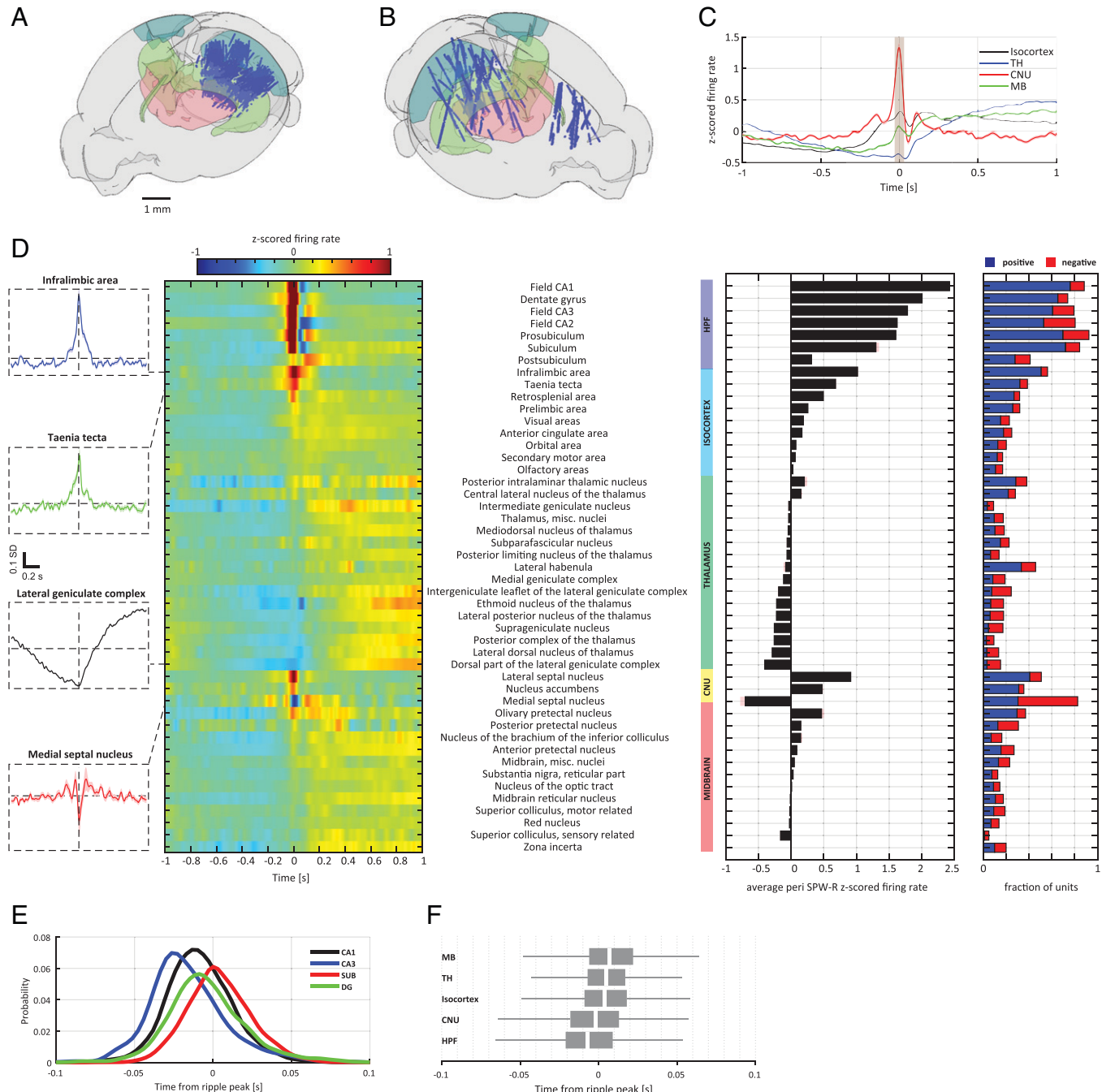


Fig. 3. Brain-wide firing rate modulation with SPW-Rs. (A) Locations of the 36,516 units (blue dots) recorded in Siegle et al. (15) ($n = 50$ mice, one session per animal). Shaded areas in cyan, green, and red depict visual cortex, hippocampus, and thalamus, respectively. (B) Same as in A for 17,354 units recorded in Steinmetz et al. (16) ($n = 19$ sessions from eight mice). (C) Average (mean \pm SEM) SPW-R-related activity for the four major extrahippocampal areas. CNU, cerebral nuclei; MB, midbrain; TH, thalamus. Shaded area corresponds to time windows within which spike responses were used to calculate SPW-R-related strengths and modulation direction (D). (D) SPW-R responses across data from both datasets combined (see also SI Appendix, Table S1). Left: Z-scored average peri-SPW-R histograms centered on SPW-R peaks. Dashed boxes show four peri-SPW-R histograms (± 1 s) from selected structures (mean \pm SEM). Middle: Bar graph showing the average response magnitude ± 30 ms around SPW-R peak, ranked separately by modulation magnitude in each brain region. Pink shaded area, SEM (not visible in most bars due to small values). Right: Fraction of significantly positively (blue) and negatively (red) modulated neurons in each structure (for neuron numbers and sessions, SI Appendix, Table S1). Note that these effects may not correspond to excitation and inhibition because the occurrence of SPW-R is often embedded in brain-state changes. HPF, hippocampal formation; SUB, subiculum; DG, dentate gyrus; misc., miscellaneous. (E) Probability distributions of the COM of principal neuron firing in the four hippocampal subregions. (F) Distributions of the COM for the four major extrahippocampal areas. misc., miscellaneous. Data are displayed as box plots representing median, lower, and upper quartiles and whiskers representing most extreme data points.

adjacency matrices for each session (Fig. 4D). From these matrices, we computed the geodesic path length (average shortest number of nodes between every two nodes) and clustering coefficient (indicating “small worldness”) (28) for each unit and each time window and averaged all units from the same

area. We observed a substantial decrease in path length surrounding SPW-R peaks for all areas (Fig. 4E). Similarly, all areas displayed a marked increase in clustering coefficient around SPW-Rs (Fig. 4F). Because MI measure is based on the temporal relationship of spikes, joined firing rate changes may

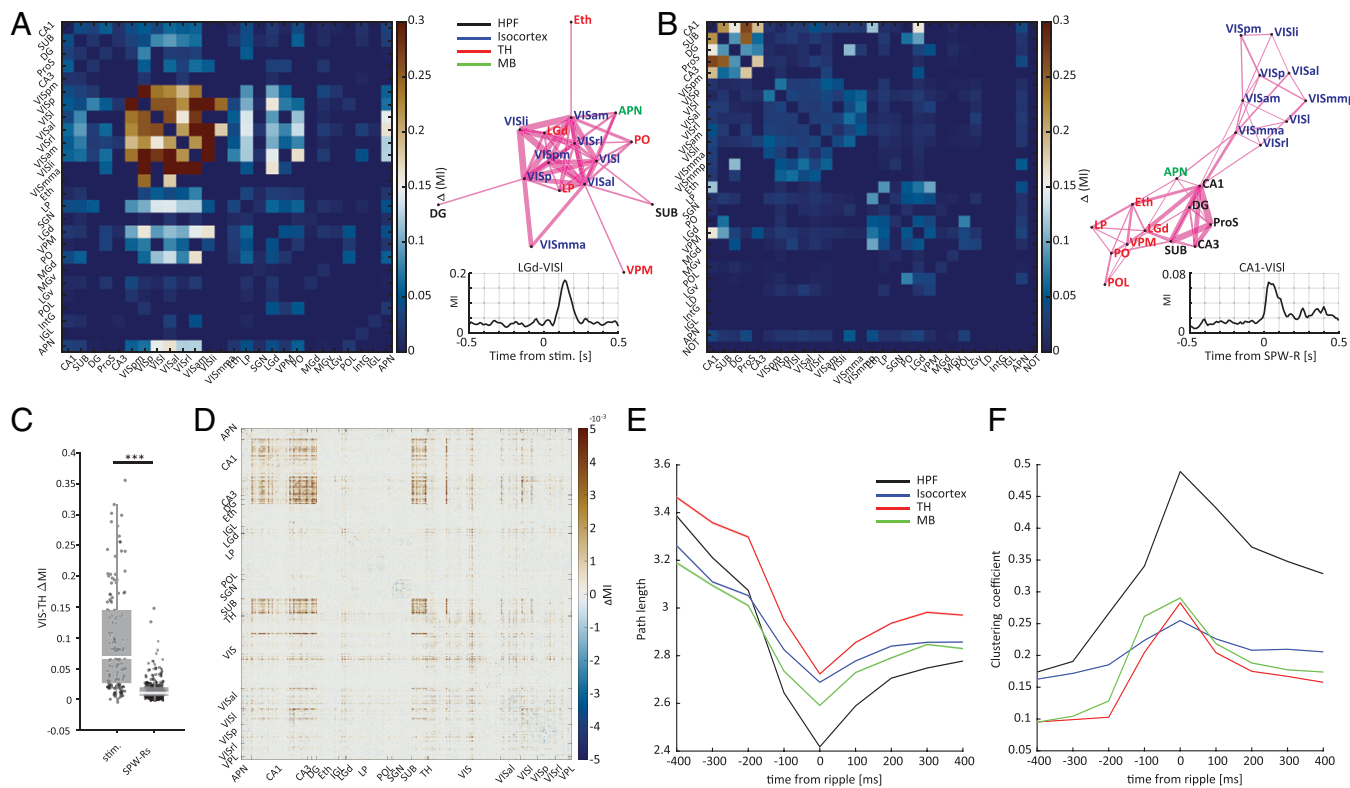


Fig. 4. SPW-Rs reorganize thalamo-cortical functional network topology. (A) *Left*: Adjacency matrix showing the increase in MI following drifting grating visual stimulation (stim.) computed between the MUA from pairs of brain areas ($n = 23$ sessions). *Right*: The corresponding undirected graph; edge thickness denotes weights. *Right Bottom*: Shows an example MI time series between LGd and a visual cortical area. (B) Same as A, but for MUA around ripple peaks ($n = 50$ sessions). (C) Distributions of ΔMI values for cortical and thalamic node pairs during either visual stimulation or SPW-Rs. Data are displayed as box plots representing median, lower and upper quartiles and whiskers representing most extreme data points ($n = 135$ and 251 pairs, respectively; *** $P = 2.5 \times 10^{-33}$, rank-sum test). (D) Example adjacency matrix ($t = 0$) of pairwise ΔMI during ripples between single units ($n = 685$) from one session. (E) Change in path length around ripples. Note the decrease across all brain areas. (F) Same as E, but for clustering coefficient. MB, midbrain; HPF, hippocampal formation; DG, dentate gyrus; SUB, subiculum; PO, posterior nucleus of the thalamus; Eth, ethmoid nucleus of the thalamus; LP, lateral posterior nucleus of the thalamus; APN, anterior pretectal nucleus; VIS, visual cortex unspecific; VISl, lateral visual area; VISli, laterointermediate area; VISam, anteromedial visual area; VISrl, rostralateral visual area; VISpm, posteromedial visual area; VISp, primary visual area; VISal, anterolateral visual area; VISmma, mediomedial anterior visual area; VISmmp, mediomedial posterior visual area; POL, posterior limiting nucleus of the thalamus; SGN, suprageniculate nucleus; TH, thalamus.

affect MI values. Despite this caveat, these findings illustrate that the spiking structure among brain areas can rapidly reorganize when the brain is disengaged from environmental inputs.

Next, we examined the relationship between the magnitude of SPW-Rs and associated spiking activity in extrahippocampal regions both before and after the emergence of SPW-Rs. In the first analysis, we calculated the spike density surrounding SPW-Rs (± 0.5 s) in each brain region separately for SPW-Rs of increasing magnitude recorded on the probe in the subiculum region (probe S). We observed that the amplitude of SPW-R covaried with spiking activity in other brain areas both before and after the occurrence of SPW-R. Unexpectedly, the temporal evolution of activity in the thalamus, midbrain, and visual cortex showed opposite trends for small- and large-amplitude SPW-Rs (Fig. 5A). Paradoxically, the largest amplitude SPW-Rs were followed by decreased spiking in all other brain areas (Fig. 5A). Similar temporal profiles were observed when we examined the relationship between the magnitude of intrahippocampal spatial synchrony of SPW-Rs and spiking activity in cortical and subcortical regions (Fig. 5B). These qualitative observations were quantified by correlating SPW-R magnitude with both pre- (-350 ms to -150 ms) and post- (-50 to 150 ms) SPW-R peak time windows of spiking activity in partner structures. Prior to SPW-Rs, spiking activity in extrahippocampal areas was positively correlated with the SPW-R amplitude, whereas surrounding the SPW-R, a negative correlation was observed (Fig. 5 C and D). While

the responses of individual units were heterogeneous, the majority of significantly modulated units in all target areas followed the population trend and decreased their firing with increasing ripple power (SI Appendix, Fig. S6). When the most posterior site was used as a reference, the differences in the pre-SPW-R epoch were less prominent, whereas the post-SPW-R suppression of spiking in extrahippocampal areas remained robust (SI Appendix, Fig. S6). This latter observation indicated that in addition to the magnitude of SPW-Rs, the intrahippocampal topographical origin of SPW-Rs was also an important factor in influencing extrahippocampal activity.

To analyze the contribution of the topographic relationship between the relative dominance of SPW-Rs in different hippocampal segments and extrahippocampal spiking further, we selected SPW-Rs detected in isolation on one of the six probes. These isolated events were generally of small amplitude. While SPW-Rs recorded at nearby sites were associated with similar midbrain, thalamic, and visual cortical patterns, comparison of SPW-Rs occurring at anterior and posterior sites showed different response profiles in these three major partner brain regions (Fig. 6A). Similarly, different response profiles were obtained when the peri-SPW-R histograms in target areas were triggered by SPW-Rs occurring at the hippocampal site with maximal ripple power, irrespective of whether SPW-Rs were present at other sites or not (Fig. 6B). We quantified these differences by comparing the session-averaged SPW-R modulation scores

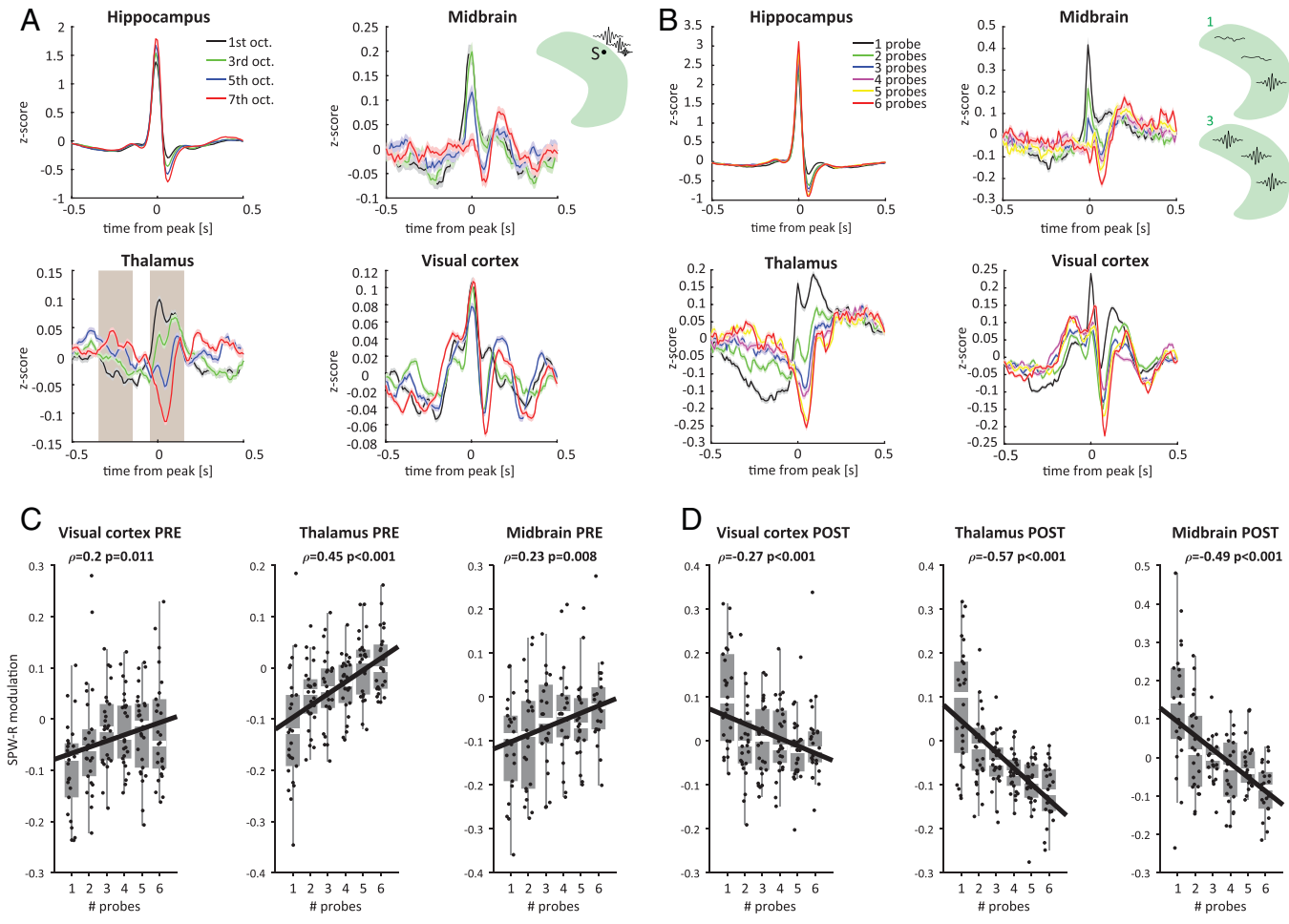


Fig. 5. SPW-R correlations with spiking activity in extrahippocampal areas vary as a function SPW-R magnitude. (A) Average peri-SPW-R spike responses from the four major brain regions, centered on the peak of ripple power. Responses for ripples of increasing power detected on the subiculum probe (probe S; see green illustration on the right; values for first, third, fifth, and seventh octiles (octs.) are shown; $n = 28,568$ units from 38 sessions where probe S was available) are shown by different colors. Shaded areas in lower Left: time windows within which spike counts in partner regions were counted before and after SPW-R. (B) Similar plot to A but here the magnitude of spatial synchrony of SPW-Rs across the hippocampal six recording sites are shown. (C) Distributions of pre-SPW-R modulations (left shaded brown area in A) across the six recording sites, averaged across all units from the same area and session. Data are displayed as box plots representing median, lower, and upper quartiles and whiskers representing most extreme data points. Linear regression lines are shown in black. Pearson's rho and p-values are indicated on top of each panel. (D) Same as C for post-SPW-R activity (right shaded brown area in A). 1st, first; oct., octile.

(mean z-scored -50 ms to 150 ms around ripple peak) for each hippocampal site and each area, yielding significant differences between septal and posterior sites (Fig. 6C).

To quantify the covariation of neuronal spiking activity at different hippocampal locations and across different brain regions, we performed principal component analysis on each region's responses. For each probe and area, the first three principal components explained more than 50% of the variability in responses. Their projections displayed qualitatively different temporal profiles for dorsal and posterior SPW-Rs (*SI Appendix*, Fig. S7). Responses to both dorsal and posterior SPW-Rs could be decomposed into both positive and negative components, suggesting heterogeneous modulation among individual neurons. However, while responses to dorsal SPW-Rs were best explained by positive lower dimensional representations, negative sign profiles were more dominant among posterior SPW-Rs. As an alternative approach (13), we compared the correlations between modulation scores to SPW-Rs on the most septal (A) and most posterior (D) sites for all extrahippocampal units in all sessions where both probes were available ($n = 34$ sessions). The correlations significantly departed from the diagonal, revealing a stronger modulation by dorsal SPW-Rs (Fig. 6D; *SI Appendix*, Fig. S7 details individual

sessions). Consistent with the stronger up-modulation of firing rates in response to septal SPW-Rs, a larger fraction of units increased their activity when referenced to probe A, while the majority of units modulated by posterior SPW-Rs decreased their firing rates (*SI Appendix*, Fig. S7). We validated these findings further by training a linear support vector machine (SVM) classifier on the firing rate vectors from all units in a given session, excluding hippocampal units, surrounding isolated dorsal and posterior region SPW-Rs. The SVM correctly classified SPW-R location above chance levels already before SPW-R onset and reached maximal accuracy around SPW-R peak (Fig. 6E). Together, these analyses indicate that ongoing activity in extrahippocampal brain areas differentially biases the timing and probability of occurrence of SPW-Rs in different hippocampal segments. In the return direction, the magnitude of SPW-Rs predicts whether neurons in the target areas increase or decrease their firing rates.

Another factor that should be taken into consideration when evaluating the interaction between hippocampus and neocortex in the waking, resting mouse is the short bouts (1 to 3 s) of 3- to 5-Hz oscillations in the visual cortex (29, 30). The results on the interaction between 4-Hz neocortical activity and SPW-Rs are summarized in *SI Appendix*, Fig. S8.

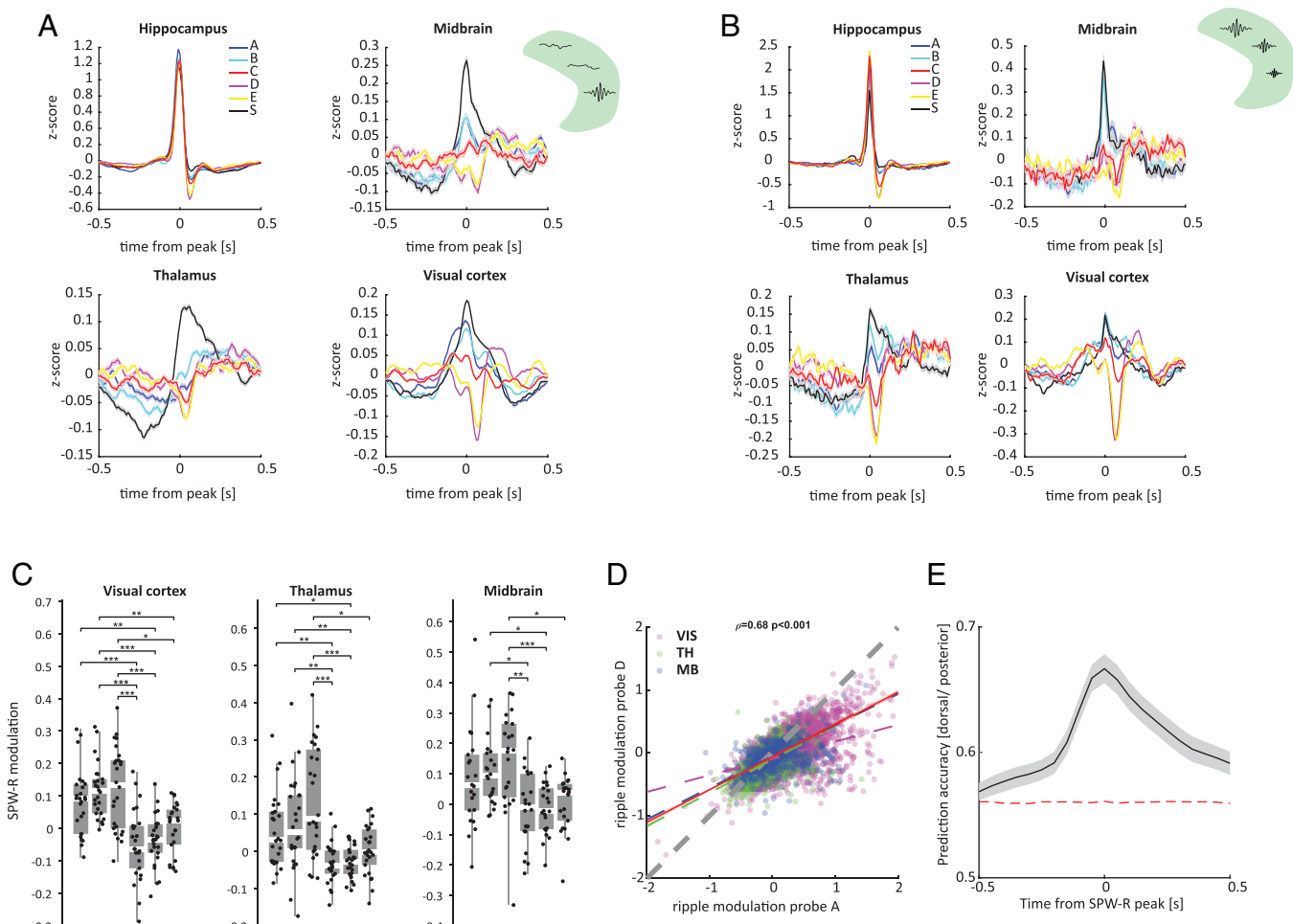


Fig. 6. SPW-R correlations with spiking activity in extrahippocampal areas vary as a function of the intrahippocampal origin of SPW-Rs. (A) Average peri-SPW-R spike responses (mean \pm SEM) from the four major brain regions, triggered on the peak of ripple power detected on different probes (illustrated by green cartoon on the right). Analysis was restricted to isolated SPW-R events (i.e., those detected on a single probe only; *Top Right* cartoon). See Fig. 1A for anatomical probe locations ($n = 36,516$ units from 50 sessions). (B) Similar display to A, but here the reference electrode was the site with the largest ripple power, irrespective of whether SPW-Rs were detected at other hippocampal sites or not. (C) Distributions of session-averaged SPW-R modulation scores across all probes for the three main areas included in the dataset ($n = 26$ sessions where all probes were available); * $P < 0.05$; ** $P < 0.01$; *** $P < 0.001$; Kruskal-Wallis test followed by Tukey-Kramer post hoc tests). Data are displayed as box plots representing median, lower and upper quartiles and whiskers representing most extreme data points. (D) Firing rate modulations of all extrahippocampal units for SPW-R detected on probe A (most dorsal probe), plotted against SPW-Rs detected on probe D (most posterior). Each dot is one unit from visual cortex (magenta), thalamus (green), or midbrain (blue). Only units that are significantly modulated on either probe A or D are shown. Red line depicts linear least square regression slope with CIs obtained from 5,000 bootstraps. Regression lines for individual areas are shown separately as dotted lines in the respective color. Gray dotted line is the unity line ($n = 10,587$ units from 34 sessions where both probes A and D were available; $P < 0.001$). *SI Appendix, Fig. S7* shows individual sessions. (E) Performance of cross-validated SVM decoder (mean \pm SEM, gray shaded area) trained to classify isolated dorsal and posterior SPW-Rs based on peri-SPW-R normalized firing rates from all extrahippocampal units in a given session ($n = 29$ sessions where probes A, B, D, and E were all simultaneously available). Red dashed line, upper 95% confidence bound obtained after 1,000 shuffles of SPW-R location labels. MB, midbrain; TH, thalamus.

Discussion

Analyzing large-scale extracellular recordings in immobile, head-fixed mice, we investigated the within-hippocampal cooperation of neuronal activity during SPW-R events and its relationship with spiking activity across the brain. We found that SPW-R-related activity spread, on average, in a temporo-septal direction and that the magnitude of SPW-Rs correlated with the spatial extent of the hippocampal population bursts. Activity surrounding SPW-Rs in extrahippocampal regions was heterogeneous and displayed a complex relationship that depended both on the magnitude of SPW-R and on the hippocampal segment in which it emerged. The magnitude and spread of SPW-Rs varied as a function of the preceding spiking activity in the neocortex, thalamus, and midbrain. In the return direction, spiking activity after SPW-Rs in extrahippocampal areas depended on

the magnitude of SPW-Rs. Both posterior and large-amplitude SPW-Rs were often associated with suppression of gross MUA in target areas. Our findings expand previous knowledge about both intrahippocampal activity and the mutual interactions between hippocampal and extrahippocampal brain circuits.

Intrahippocampal Synchrony During SPW-Rs. In the rat, SPW-Rs occur at every segment of the septotemporal axis of the CA1 region, and the locally generated ripple events are qualitatively similar (14, 31). Our findings in the mouse confirm these observations. We found a reliable relationship between the sharp wave amplitude, ripple magnitude and duration, and spatial synchrony of SPW-R events. While small-amplitude events remained relatively local, large-amplitude SPW-Rs occurred synchronously over larger distances.

Previous work in rats and monkeys indicated large variability of SPW-R patterns (14, 31, 32). One potential source of local variability is the direction of travel and the intrahippocampal amplification of population events. In our dataset, a minority of events were confined to a single site, whereas most SPW-Rs were synchronous across all six electrodes spanning from the septal to the posterior segments of the hippocampus. One likely source of propagation of SPW-Rs is the extensive recurrent collaterals of the CA3 neurons (33, 34). Accordingly, each SPW-R event is a sweep in space, whereas individual ripple waves reflect local interactions between CA1 pyramidal cells and interneurons. In support of this model, optogenetic stimulation, mimicking sharp wave–induced depolarization of a local group of CA1 neurons by their upstream CA3 partners, induce ripple-like patterns, which rarely propagate in the CA1 plane (35). Yet, the CA1 circuit can further boost population synchrony, as was revealed here by the steeper slope between ripple power magnitude and the larger fraction of SPW-R–participating neurons in CA1 compared to the CA3 region (21).

Supporting previous reports, both the incidence and magnitude (hence spatial synchrony) of SPW-Rs varied with global brain-state measures, such as pupil size and the slope of the power spectrum (18, 19), indicating that SPW-Rs both affect and are affected by activity in other brain areas (6, 36). It is important to emphasize that the spatial coverage of the hippocampus in our dataset was confined to septal to posterior (or intermediate) hippocampus and may not generalize to the ventral third (13), from which no recordings were available.

Reciprocal SPW-R-Mediated Communication With Cortical and Subcortical Brain Regions. Most previous experiments compared physiological features of SPW-Rs to activity in a single other cortical or subcortical region, and studies relating SPW-Rs to neocortical topography are rare (7, 11). A prominent exception is the pioneering imaging work of Logothetis et al. (6), which analyzed SPW-R-centered BOLD activity in the entire brain of monkeys. In those experiments, most of the cerebral cortex was “activated” during the SPW-Rs, whereas most diencephalic, midbrain, and brainstem regions were suppressed. The authors hypothesized that the occurrence of SPW-Rs corresponds to privileged time windows when internal communication between hippocampus and neocortex is enhanced, whereas sensory influences, mediated by the thalamocortical paths, are suppressed. Our findings are in support of the hypothesis that internalized communication is enhanced during SPW-Rs at the expense of attending to the environment. For example, during visual stimulation, neurons in visual cortex and thalamus formed tight clusters with each other (“sensory processing”). In contrast, functional connectivity between the hippocampus and visual areas increased during SPW-Rs (“internal processing”).

Yet, our conclusions about interregional interactions are different from those suggested in the imaging study (6). A large part of the difference may be due to the differences between spike-based and BOLD signal–based inferences about neuronal activity (6). The higher temporal resolution afforded by the electrophysiological signals allowed us to distinguish neuronal interactions at the tens of milliseconds versus seconds time scales in functional MRI. When longer time scale interactions are considered, corresponding to the resolution of the BOLD signal, our results are in apparent agreement with the inferences of Logothetis et al. (6). Activities integrated both before and after SPW-R occurrence, on average, showed increased activity in cortical areas, whereas spiking in the thalamus was largely diminished. However, examination of the multiple relationships

at the physiologically relevant short-time scale revealed a different picture. Target areas monosynaptically connected to the hippocampus, such as the infralimbic prefrontal cortex (22), retrosplenial cortex (12, 23), cingulate cortex (37), and taenia tecta showed short-latency activation centered around SPW-Rs. Similarly, subcortical structures, including the lateral septum (38), nucleus accumbens (39), and selected pretectal midbrain nuclei, were also activated by SPW-Rs at a short latency, whereas average responses in the medial septum, which is innervated by the terminals of long-range hippocampo-septal inhibitory interneurons (40), were suppressed (41). These short-latency effects were significantly correlated with the density of hippocampal fiber projections to these structures.

Unlike the transient short-time scale responses, average population responses from the majority of recorded regions shared a common longer time scale modulation, upon which the SPW-R–induced short-time scale responses appeared superimposed. Integrated activity was low prior to the SPW-R and steadily increased thereafter. This interregionally shared neuronal behavior is reminiscent of the DOWN-to-UP state change in spiking activity during non–rapid eye movement sleep (42), even though the mice did not fall asleep during the short recording sessions (15). Yet, several recent papers pointed out that population silence of neurons (definition of the DOWN state) can also occur during resting immobility states in both rodents and humans (12, 20, 43). Previous studies have already demonstrated that SPW-Rs can induce DOWN states in the prefrontal region (22, 44) and that DOWN-UP shifts in other regions coincide significantly with hippocampal SPW-Rs (45–50). Overall, our findings imply that SPW-Rs are embedded in global brain-state changes, increasing their probability of occurrence at such state transitions (51) and, in return, can trigger either relatively localized or more global brain-state changes.

Topographic and Magnitude Effects of SPW-Rs. A loose topographic organization exists between different segments of the hippocampus and the neocortex. Outputs from the dorsal and posterior/ventral parts of the hippocampus are routed by way of the retrosplenial cortex and entorhinal cortex, respectively (52, 53). The septal hippocampus is more strongly connected to the (dorso-)medial entorhinal cortex and the postrhinal cortex (rodent homolog of the parahippocampal cortex in primates), whereas the ventral hippocampus, lateral entorhinal cortex, and perirhinal cortex form a relatively independent stream (54). In turn, the parahippocampal cortex communicates mainly with the “default network” (55), while the perirhinal cortex has stronger connections to the lateral orbitofrontal cortex and the anterior ventrolateral temporal cortex (54). Further, there is a reciprocal topographic relationship between neocortex–entorhinal cortex–hippocampus anatomical organization (56). The dataset we analyzed did not allow us to address the functional consequences of these topographical relationships in detail, even though experiments in both rodents and humans show that SPW-Rs can route the hippocampal output to unique brain targets depending on the nature of information to be remembered (11, 23, 56, 57). Similar to the propagating SPW-Rs in the hippocampus, both UP-DOWN slow oscillations and sleep spindles show a traveling wave pattern in the neocortex (58–61). As a consequence, SPW-R incidence and magnitude should vary as a function of the UP-DOWN event phase, depending on the location of the reference neocortical site. In line with this hypothesis, SPW-Rs in the dorsal hippocampus are best correlated with the UP→DOWN state transition in the prefrontal cortex (22, 44),

whereas the entorhinal cortex is most strongly correlated with UP states or the DOWN→UP state transition (62). In further support of this hypothesized relationship, in which neocortical and hippocampal patterns track each other in time and space, we found that SPW-Rs at different CA1 locations coincided with different phases of slowly changing firing rates in the midbrain, thalamus and visual cortex.

Examination of the dependency of firing rate changes in extrahippocampal brain areas on SPW-R spatial synchrony and magnitude revealed an unexpected relationship. Small-amplitude SPW-R events were preceded by initial low firing rates in extrahippocampal areas and correlated with increased spiking activity prior to and around SPW-R time. In contrast, large-amplitude SPW-R events were followed by a strong decrease of spiking in all recorded partner structures. These observations can be explained by the ability of strongly synchronous SPW-Rs to trigger UP→DOWN transitions in the neocortex, possibly mediated by the entorhinal (62) and/or retrosplenial (12) cortices. Based on these findings, we hypothesize that elevated inputs to the hippocampus, for example, during DOWN-UP transitions, will increase the likelihood of SPW-R occurrence (35). In turn, when multiple local SPW-Rs are combined spatially, the large-amplitude SPW-Rs can effectively terminate the ongoing cortical activity, resulting in a DOWN state (51, 63). In contrast, weak hippocampal outputs may operate below a critical threshold for inducing a state transition. Alternatively, variations in the magnitude of SPW-Rs and associated extrahippocampal pattern changes may be brought about by changes in subcortical inputs to the hippocampus (64, 65). Future perturbation experiments manipulating both cortical and subcortical inputs to the hippocampus will be required to address the directional effects. It also remains to be tested whether the relationship between SPW-R magnitude and origin and firing rate changes in extrahippocampal regions holds true for nonvisual areas, which were the main focus of our investigation. In summary, an important implication of these

findings is that increased and decreased firing rates in target areas after SPW-Rs cannot be equated with excitation and inhibition, respectively, because of the simultaneously occurring state changes.

Materials and Methods

For all analyses presented in the paper, we use data from the Allen Brain Institute Visual Coding dataset publicly available at https://allenSDK.readthedocs.io/en/latest/visual_coding_neuropixels.html or the Steinmetz et al. (16) data, available at https://figshare.com/articles/dataset/Eightprobe_Neuropixels_recordings_during_spontaneous_behaviors/7739750. SPW-R detection was restricted to epochs where the speed of the animal was below 2 cm/s for at least 2 s. Putative SPW-R events were defined as those where the beginning/end cutoffs exceeded 2 SDs and the peak power 3 SDs. Ripple-triggered PETHs were computed by counting spiking activity around peak ripple time into 1-ms (Fig. 3) or 10-ms bins (Figs. 5 and 6). For predicting the hippocampal origin of SPW-Rs, we used a linear SVM trained using 10-fold cross validation. Decoding accuracy is reported as the mean of the cross-validated accuracy. To obtain CIs, we randomly shuffled the data labels 1,000 times. Details of analyses are presented in *SI Appendix*.

Data Availability. Code, AI data (15), and UCL data (16) have been deposited in GitHub, FMAT Toolbox, Allen SDK, and Figshare. The code used for this study was adapted from the buzcode repository (<https://github.com/buzsakilab/buzcode>) and the FMAT toolbox (<http://fmatoolbox.sourceforge.net/>). The AI data are available at https://allenSDK.readthedocs.io/en/latest/visual_coding_neuropixels.html. The UCL data are available at https://figshare.com/articles/dataset/Dataset_from_Steinmetz_et_al_2019/9598406. All study data are included in the article and/or *SI Appendix*. Previously published data were used for this work (15, 16).

ACKNOWLEDGMENTS. We thank the AI (15) and Steinmetz and colleagues (16) for making the datasets available. We thank Roman Huszar, Mihály Vöröslakos, and Manuel Valero for comments and feedback on the manuscript. This work was supported by NIH Grant Nos. MH107396, U19 NS107616, and U19 NS104590 and the DFG Exc 2049 and SFB 1315 (Grant No. 390688087). N.N. is supported by a DFG Walter Benjamin stipend.

1. G. Buzsáki, Neural syntax: Cell assemblies, synapsembles, and readers. *Neuron* **68**, 362–385 (2010).
2. E. V. Lubenov, A. G. Siapas, Hippocampal theta oscillations are travelling waves. *Nature* **459**, 534–539 (2009).
3. J. Patel, S. Fujisawa, A. Berényi, S. Royer, G. Buzsáki, Traveling theta waves along the entire septotemporal axis of the hippocampus. *Neuron* **75**, 410–417 (2012).
4. R. A. Swanson, D. Levenstein, K. McClain, D. Tingley, G. Buzsáki, Variable specificity of memory trace reactivation during hippocampal sharp wave ripples. *Curr. Opin. Behav. Sci.* **32**, 126–135 (2020).
5. G. Buzsáki, D. Tingley, Space and time: The hippocampus as a sequence generator. *Trends Cogn. Sci.* **22**, 853–869 (2018).
6. N. K. Logothetis *et al.*, Hippocampal-cortical interaction during periods of subcortical silence. *Nature* **491**, 547–553 (2012).
7. J. Karimi Abadchi *et al.*, Spatiotemporal patterns of neocortical activity around hippocampal sharp-wave ripples. *eLife* **9**, 1–26 (2020).
8. N. K. Logothetis, What we can do and what we cannot do with fMRI. *Nature* **453**, 869–878 (2008).
9. G. Buzsáki, Hippocampal sharp wave-ripple: A cognitive biomarker for episodic memory and planning. *Hippocampus* **25**, 1073–1188 (2015).
10. X. Liu *et al.*, Multimodal neural recordings with Neuro-FITM uncover diverse patterns of cortical-hippocampal interactions. *Nat. Neurosci.* **24**, 886–896 (2021).
11. Y. Norman, O. Raccah, S. Liu, J. Parvizi, R. Malach, Hippocampal ripples and their coordinated dialogue with the default mode network during recent and remote recollection. *Neuron* **109**, 2767–2780.e5 (2021).
12. N. Nitzan *et al.*, Propagation of hippocampal ripples to the neocortex by way of a subiculum-retrosplenial pathway. *Nat. Commun.* **11**, 1–17 (2020).
13. M. Sosa, H. R. Joo, L. M. Frank, Dorsal and ventral hippocampal sharp-wave ripples activate distinct nucleus accumbens networks. *Neuron* **105**, 725–741.e8 (2020).
14. J. Patel, E. W. Schomburg, A. Berényi, S. Fujisawa, G. Buzsáki, Local generation and propagation of ripples along the septotemporal axis of the hippocampus. *J. Neurosci.* **33**, 17029–17041 (2013).
15. J. H. Siegle *et al.*, Survey of spiking in the mouse visual system reveals functional hierarchy. *Nature* **592**, 86–92 (2021).
16. N. A. Steinmetz, P. Zatka-Haas, M. Carandini, K. D. Harris, Distributed coding of choice, action and engagement across the mouse brain. *Nature* **576**, 266–273 (2019).
17. K. Mizuseki, K. Diba, E. Pastalkova, G. Buzsáki, Hippocampal CA1 pyramidal cells form functionally distinct sublayers. *Nat. Neurosci.* **14**, 1174–1181 (2011).
18. M. J. McGinley, S. V. David, D. A. McCormick, Cortical membrane potential signature of optimal states for sensory signal detection. *Neuron* **87**, 179–192 (2015).
19. R. Gao, E. J. Peterson, B. Voytek, Inferring synaptic excitation/inhibition balance from field potentials. *Neuroimage* **158**, 70–78 (2017).
20. A. Luczak, P. Bartho, K. D. Harris, Gating of sensory input by spontaneous cortical activity. *J. Neurosci.* **33**, 1684–1695 (2013).
21. J. Csicsvari, H. Hirase, A. Mamiya, G. Buzsáki, Ensemble patterns of hippocampal CA3-CA1 neurons during sharp wave-associated population events. *Neuron* **28**, 585–594 (2000).
22. A. Peyrache, M. Khamassi, K. Benchenane, S. I. Wiener, F. P. Battaglia, Replay of rule-learning related neural patterns in the prefrontal cortex during sleep. *Nat. Neurosci.* **12**, 919–926 (2009).
23. D. Khodagholy, J. N. Gelinas, G. Buzsáki, Learning-enhanced coupling between ripple oscillations in association cortices and hippocampus. *Science* **358**, 369–372 (2017).
24. J. de Olmos, H. Hardy, L. Heimer, The afferent connections of the main and the accessory olfactory bulb formations in the rat: An experimental HRP-study. *J. Comp. Neurol.* **181**, 213–244 (1978).
25. M. B. Luskin, J. L. Price, The topographic organization of associational fibers of the olfactory system in the rat, including centrifugal fibers to the olfactory bulb. *J. Comp. Neurol.* **216**, 264–291 (1983).
26. D. Sullivan *et al.*, Relationships between hippocampal sharp waves, ripples, and fast gamma oscillation: Influence of dentate and entorhinal cortical activity. *J. Neurosci.* **31**, 8605–8616 (2011).
27. N. M. Timme, C. Lapish, A tutorial for information theory in neuroscience. *eNeuro* **5**, ENEURO.0052-18.2018 (2018).
28. D. J. Watts, S. H. Strogatz, Collective dynamics of 'small-world' networks. *Nature* **393**, 440–442 (1998).
29. M. C. Einstein, P.-O. Polack, D. T. Tran, P. Golshani, Visually evoked 3–5 Hz membrane potential oscillations reduce the responsiveness of visual cortex neurons in awake behaving mice. *J. Neurosci.* **37**, 5084–5098 (2017).
30. Y. Senzel, A. Fernandez-Ruiz, G. Buzsáki, Layer-specific physiological features and interlaminar interactions in the primary visual cortex of the mouse. *Neuron* **101**, 500–513.e5 (2019).
31. J. Taxidis, C. A. Anastassiou, K. Diba, C. Koch, Local field potentials encode place cell ensemble activation during hippocampal sharp wave ripples. *Neuron* **87**, 590–604 (2015).
32. J. F. Ramirez-Villegas, N. K. Logothetis, M. Besserve, Diversity of sharp-wave-ripple LFP signatures reveals differentiated brain-wide dynamical events. *Proc. Natl. Acad. Sci. U.S.A.* **112**, E6379–E6387 (2015).
33. X.-G. Li, P. Somogyi, A. Ylinen, G. Buzsáki, The hippocampal CA3 network: An in vivo intracellular labeling study. *J. Comp. Neural.* **339**, 181–208 (1994).
34. N. Ishizuka, J. Weber, D. G. Amaral, Organization of intrahippocampal projections originating from CA3 pyramidal cells in the rat. *J. Comp. Neurol.* **295**, 580–623 (1990).
35. E. Stark *et al.*, Pyramidal cell-interneuron interactions underlie hippocampal ripple oscillations. *Neuron* **83**, 467–480 (2014).

36. G. Buzsáki, The hippocampo-neocortical dialogue. *Cereb. Cortex* **6**, 81–92 (1996).
37. D. V. Wang, S. Ikemoto, Coordinated interaction between hippocampal sharp-wave ripples and anterior cingulate unit activity. *J. Neurosci.* **36**, 10663–10672 (2016).
38. D. Tingley, G. Buzsáki, Routing of hippocampal ripples to subcortical structures via the lateral septum. *Neuron* **105**, 138–149.e5 (2020).
39. L. Sjulson, A. Peyrache, A. Cumpelik, D. Cassataro, G. Buzsáki, Cocaine place conditioning strengthens location-specific hippocampal coupling to the nucleus accumbens. *Neuron* **98**, 926–934.e5 (2018).
40. A. I. Gulyás, N. Hájos, I. Katona, T. F. Freund, Interneurons are the local targets of hippocampal inhibitory cells which project to the medial septum. *Eur. J. Neurosci.* **17**, 1861–1872 (2003).
41. G. Dragoi, D. Carpi, M. Recce, J. Csicsvari, G. Buzsáki, Interactions between hippocampus and medial septum during sharp waves and theta oscillation in the behaving rat. *J. Neurosci.* **19**, 6191–6199 (1999).
42. M. Steriade, D. A. McCormick, T. J. Sejnowski, Thalamocortical oscillations in the sleeping and aroused brain. *Science* **262**, 679–686 (1993).
43. Y. Nir *et al.*, Regional slow waves and spindles in human sleep. *Neuron* **70**, 153–169 (2011).
44. J. N. Gelinas, D. Khodagholy, T. Thesen, O. Devinsky, G. Buzsáki, Interictal epileptiform discharges induce hippocampal-cortical coupling in temporal lobe epilepsy. *Nat. Med.* **22**, 641–648 (2016).
45. A. G. Siapas, M. A. Wilson, Coordinated interactions between hippocampal ripples and cortical spindles during slow-wave sleep. *Neuron* **21**, 1123–1128 (1998).
46. F. P. Battaglia, G. R. Sutherland, B. L. McNaughton, Hippocampal sharp wave bursts coincide with neocortical “up-state” transitions. *Learn. Mem.* **11**, 697–704 (2004).
47. A. Sirota, J. Csicsvari, D. Buhl, G. Buzsáki, Communication between neocortex and hippocampus during sleep in rodents. *Proc. Natl. Acad. Sci. U.S.A.* **100**, 2065–2069 (2003).
48. A. Sirota *et al.*, Entrainment of neocortical neurons and gamma oscillations by the hippocampal theta rhythm. *Neuron* **60**, 683–697 (2008).
49. M. Mölle, O. Yeschenko, L. Marshall, S. J. Sara, J. Born, Hippocampal sharp wave-ripples linked to slow oscillations in rat slow-wave sleep. *J. Neurophysiol.* **96**, 62–70 (2006).
50. M. Yang, N. K. Logothetis, O. Eschenko, Occurrence of hippocampal ripples is associated with activity suppression in the mediodorsal thalamic nucleus. *J. Neurosci.* **39**, 434–444 (2019).
51. D. Levenstein, G. Buzsáki, J. Rinzel, NREM sleep in the rodent neocortex and hippocampus reflects excitable dynamics. *Nat. Commun.* **10**, 1–12 (2019).
52. G. D. Petrovich, N. S. Canteras, L. W. Swanson, Combinatorial amygdalar inputs to hippocampal domains and hypothalamic behavior systems. *Brain Res. Rev.* **38**, 247–289 (2001).
53. M. P. Witter, H. J. Groenewegen, F. H. Lopes da Silva, A. H. M. Lohman, Functional organization of the extrinsic and intrinsic circuitry of the parahippocampal region. *Prog. Neurobiol.* **33**, 161–253 (1989).
54. C. Ranganath, M. Ritchey, Two cortical systems for memory-guided behaviour. *Nat. Rev. Neurosci.* **13**, 713–726 (2012).
55. M. E. Raichle *et al.*, A default mode of brain function. *Proc. Natl. Acad. Sci. U.S.A.* **98**, 676–682 (2001).
56. D. G. Amaral, P. Lavanex, *The Hippocampus Book* (Oxford University Press, 2007).
57. A. P. Vaz, S. K. Inati, N. Brunel, K. A. Zaghloul, Coupled ripple oscillations between the medial temporal lobe and neocortex retrieve human memory. *Science* **363**, 975–978 (2019).
58. L. Muller *et al.*, Rotating waves during human sleep spindles organize global patterns of activity that repeat precisely through the night. *eLife* **5**, e17267 (2016).
59. L. Muller, F. Chavane, J. Reynolds, T. J. Sejnowski, Cortical travelling waves: Mechanisms and computational principles. *Nat. Rev. Neurosci.* **19**, 255–268 (2018).
60. M. Massimini, R. Huber, F. Ferrarelli, S. Hill, G. Tononi, The sleep slow oscillation as a traveling wave. *J. Neurosci.* **24**, 6862–6870 (2004).
61. Z. W. Davis, L. Muller, J. Martinez-Trujillo, T. Sejnowski, J. H. Reynolds, Spontaneous travelling cortical waves gate perception in behaving primates. *Nature* **587**, 432–436 (2020).
62. Y. Isomura *et al.*, Integration and segregation of activity in entorhinal-hippocampal subregions by neocortical slow oscillations. *Neuron* **52**, 871–882 (2006).
63. M. V. Sanchez-Vives, D. A. McCormick, Cellular and network mechanisms of rhythmic recurrent activity in neocortex. *Nat. Neurosci.* **3**, 1027–1034 (2000).
64. D. V. Wang *et al.*, Mesopontine median raphe regulates hippocampal ripple oscillation and memory consolidation. *Nat. Neurosci.* **18**, 728–735 (2015).
65. Y. Zhang *et al.*, Cholinergic suppression of hippocampal sharp-wave ripples impairs working memory. *Proc. Natl. Acad. Sci. U.S.A.* **118**, e201643211 (2021).